Time Marching Algorithm for Predicting the Linear Rheology of Monodisperse Comb Polymer Melts

ARTICLE *in* MACROMOLECULES · FEBRUARY 2011

Impact Factor: 5.8 · DOI: 10.1021/ma102041h

6 AUTHORS, INCLUDING:

Mostafa Ahmadi
Amirkabir University of Technology
25 PUBLICATIONS **142** CITATIONS
SEE PROFILE

Christian Bailly
Université catholique de Louvain
178 PUBLICATIONS **2,597** CITATIONS
SEE PROFILE

Mehdi Nekoomanesh
Iran Polymer and Petrochemical Institute
99 PUBLICATIONS **607** CITATIONS
SEE PROFILE

Evelyne van Ruymbeke
Université catholique de Louvain
40 PUBLICATIONS **710** CITATIONS
SEE PROFILE

Macromolecules
ARTICLE

Macromolecules **2011**, *44*, 647–659 **647**
DOI: 10.1021/ma102041h

Time Marching Algorithm for Predicting the Linear Rheology of Monodisperse Comb Polymer Melts

Mostafa Ahmadi,[†,§] Christian Bailly,[†] Roland Keunings,[‡] Mehdi Nekoomanesh,[§] Hassan Arabi,[§] and Evelyne van Ruymbeke*[,†]

[†]*Bio and Soft Matter, Institute of Condensed Matter and Nano-science, Université Catholique de Louvain, Louvain-la-Neuve, Belgium,* [‡]*Louvain School of Engineering, ICTEAM Institute, Université Catholique de Louvain, Louvain-la-Neuve, Belgium, and* [§]*Polymerization Group, Engineering Department, Iran Polymer and Petrochemical Institute, Tehran, Iran*

Received September 2, 2010; Revised Manuscript Received December 10, 2010

ABSTRACT: We extend van Ruymbeke et al.'s time marching algorithm (TMA) (*Macromolecules* **2006**, *39*, 6248) in order to predict the linear viscoelastic properties of comb polymer melts. While former tube models have shown limitations for predicting the relaxation of comb polymer with short side branches, we observe here a good agreement between predictions and the experimental data for both combs with long and short side branches. In order to determine the origin of this improvement, we study the influence of the different elements present in the TMA model. In particular, we show the importance of taking into account the monomeric friction coming from the backbone itself in the total drag of the molecule, considering the modification of early time fluctuations and introducing the tube dilation process as a continuous function evolving through time. Then, based on a wide range of experimental data on different comb structures, we explore the limits of the relaxation behavior that comb polymers can show. If the friction from the relaxed side branches is significant, the backbone segments seem to fluctuate with respect to the closest branching point, just like a Cayley-tree molecule. On the other hand if the extra friction is negligible in comparison to the potential barrier of retraction along the backbone, the segments fluctuate with respect to the middle of the molecule, just like a linear chain.

I. Introduction

One of the important objectives of polymer rheology is to relate the microstructure of macromolecules to their macroscopic flow behavior. The original picture of stress relaxation in a tube defined by topological constraints from neighboring chains has yielded fundamental results in this direction.[1,2] In the framework of tube models, linear chains mainly relax their orientation by curvilinear diffusion along the confining tube. This is called reptation. However, reptation is unlikely for stars due to anchoring effect of the branching point. Stars have to relax their orientation by entropically unfavorable retraction along the tube toward the branching point,[3−5] which is called fluctuations. When relaxation by fluctuations spans a wide time scale, relaxed segments can be considered as solvent for oriented ones. They accelerate relaxation by reducing entanglement density, which is called dynamic tube dilation (DTD).[6,7] Combining the processes mentioned above enables quantitative predictions of experimental linear viscoelastic (LVE) properties for simple and even complex architectures.[8,9]

Tube-based models have now become mature enough to yield excellent LVE predictions for model architectures such as asymmetric star,[10,11] H-shaped,[12] pom-pom,[13,14] Cayley-tree,[15,16] "branch on branch"[17−19] macromolecules, and even supra-molecular structures.[20] The key concept is that complex molecules relax hierarchically in the framework of DTD.[17−22] In other words, stress relaxation starts from the outer parts such as the free ends of dangling branches and ends up at the most constrained inner parts of the molecule. The relaxed outer parts yield more friction for relaxation of inner segments while they make the tube dilated by acting as solvent according to the DTD picture.

*Corresponding author. E-mail: evelyne.vanruymbeke@uclouvain.be.

On the basis of the success of the hierarchical relaxation concept for predicting the relaxation of H-shaped and pom-pom polymers, application of this idea to comb structures has been the subject of several publications.[23−29] A model comb chain consists of a linear backbone with randomly distributed branches of equal length. Stress relaxation starts by retraction of the branches and backbone free ends, generating a star-like signature at high frequencies. This is followed by slow fluctuations of the oriented backbone along a dilated tube, subject to the extra friction from relaxed branches. As the final relaxation process, reptation of the backbone can occur.[21] This model has been applied to different classes of lightly and heavily branched combs by Daniels et al.[23] The input parameters of their model belong to three categories: (i) the chemistry dependent parameters, i.e. the entanglement molecular weight, M_e, the plateau modulus, G_N^0, and characteristic Rouse time of an entanglement, τ_e; (ii) the tube model parameters, i.e., the dilution exponent, α and the branch point hopping fraction, p^2; (iii) the structural parameters, i.e., the backbone length, the length and the number of branches. In order to obtain good predictions when keeping the fundamental tube parameters α and p^2 constant, Daniels et al. had to make minor adjustments of the chemistry dependent parameters and to fit the structural parameters. Inkson et al. have used a modified version of this model to describe rheology of monodisperse polybutadiene combs and managed to explain the complexity of experimentally determined zero-shear rate viscosity of various polyethylene combs.[24]

The model developed by Kapnistos et al. by minor modification of the previous models can successfully predict the LVE behavior of combs with long branches but shows shortcomings in the case of combs with short, i.e., unentangled or barely entangled, branches.[25] The same model was recently used by Kirkwood et al., who confirmed that it cannot correctly predict the behavior of

Published on Web 01/10/2011

combs with short branches, yielding the suggestion that such branches cause more drag than expected from tube models.[28] This idea is further supported by two additional findings: (i) the unreasonably low branch hopping fraction parameter p^2 that must be used for asymmetric stars with a short third arm, as found by Frischknecht et al.[11] and (ii) coarse-grained simulations of branch point motion in asymmetric stars by Zhou and Larson.[30] Recent neutron spin echo spectroscopy measurements of branch point motion of similar asymmetric stars published by Zamponi et al. also show that the branch point is immobile on the time scale of the experiment while the traditional tube models predict unentangled short arms should be able to move along the tube made by the two long arms at that time scale.[31]

Recently, the time marching algorithm (TMA) developed by van Ruymbeke et al. has been successfully applied to a wide range of macromolecular architectures, namely, asymmetric stars, H-shaped, pom-pom, Cayley-tree and has been extended to supra-molecular structures.[13−17,32] The TMA model is based on the same mesoscopic description of relaxation mechanisms as traditional tube-based models. However, as opposed to the latter, it follows the relaxation of molecules on a discretized time axis and can thus handle all interrelated events simultaneously, such as reptation, fluctuations, constraint release Rouse motion, and dynamic tube dilation, without the need for an artificial separation of time scales. DTD can be considered conveniently using an extended Graessley criterion. Moreover, there is no need to fit an additional branch point hopping fraction parameter p^2. Since the value of p^2 is uncertain, we prefer fixing it as equal to 1 in the TMA model. This simple approach has been shown already to give excellent results for a wide variety of architectures. The idea of removing time-scale separation between fluctuations and reptation mechanisms by use of product of these relaxation probabilities has been also successfully used by Pattamaprom et al. in the dual-constraint model.[33−35]

The objective of this paper is to extend the TMA model, including recent modifications,[36] to comb structures and confront the results to three published sets of rheological data on polystyrene (PS), polybutadiene (PBd) and polyisoperene (PI) combs.[25,28,29,37] The success of this comparison confirms the universal validity of the TMA model for complex architectures and its applicability to molecules with short dangling branches. One of our goals is to find out the origin of discrepancies between the predictions of former models and experimental LVE data on such systems.

Thus, the paper is organized as follows. Section II describes in detail the modifications of the TMA model needed to describe comb structures. Section III presents the results of the comparison between the model predictions and experimental data for three sets of polymers. Section IV provides some conclusions and perspectives.

II. Theory

Following a careful definition of the chosen segmental coordinate system for the comb architectures, we first describe the general structure of the model. Next, we detail all the relevant relaxation mechanisms for combs, i.e. branch fluctuations, backbone fluctuations and backbone reptation. The treatment of high frequency Rouse motions and early fluctuations is further described.

II.1. Definition of Coordinate System. As the segmental fluctuation times are exponentially dependent on the square of their depth and the unrelaxed fraction, the final predictions strongly depend on the detailed definition of branch and effective backbone segments. Here, we assume that q branches with the same mass M_a (see Figure 1.a, the bright lines) are uniformly distributed along the *real* backbone (i.e., as defined from the synthesis), which has a mass M_b (Figure 1a). Thus, we assume that each segment between two branching points or between a backbone extremity and the nearest branching point has a molecular weight $M_{segment}$ equal to $M_b/(q+1)$. However, in order to simplify the modeling, an *effective* backbone (*eb*) is used, as highlighted in Figure 1b, and which is defined as the longest end-to-end path of the molecule. Thus, it contains the inner part of the *real* backbone plus the longer branches fixed to the first and the last branching points (and with a mass $= \max(M_a, M_{segment})$). Using this backbone definition, two kinds of side branches (i.e., fixed on the effective backbone) must be defined (see Figure 1.b): $(q-2)$ branches with a molecular weight equal to M_a, and the two outer branches, fixed to the first and the last branching points, and which can be shorter than the other side-branches. Indeed, their molecular weight is equal to $M_{sb} = \min(M_a, M_{segment})$. Note that for comb polymers with only few short branches along the backbone, i.e with $M_a < M_{segment}$, these two outer short branches have the same length than the other side-branches ($M_a = M_{sb}$), which represents a particular case of the general definition proposed here. In addition to these two kinds of side-branches, the free ends of the *effective* backbone can also be seen as branches. Having a molecular weight equal to $\max(M_a, M_{segment})$, they are always longer or equal to the side-branches., and therefore, can be called "long branches". Using an effective backbone is motivated by the fact that the extra friction coming from the relaxed side branches is exponentially dependent on the branch length, so it is faster for the backbone to relax along the longer path in order to experience less extra friction coming from relaxed side branches.[25] The corresponding volumetric fractions of the effective backbone, the (normal) branches and the short branches are defined as

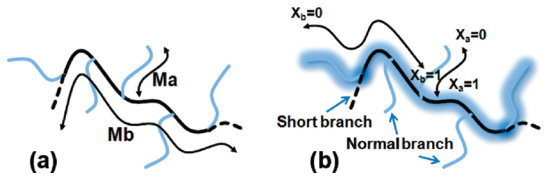

Figure 1. Definition of the coordinate system; (a) backbone's inner part (dark bold line), short branches, sb (dark dashed lines) and normal branches (bright lines) and (b) definition of the effective backbone, eb (highlighted), with $M_{eb} = (q-1)M_{segement} + 2\max(M_a, M_{segment})$.

$$\varphi_{eb} = ((q-1)M_{segment} + 2\max(M_a, M_{segment}))/(M_b + qM_a) \quad (1)$$

$$\varphi_a = (q-2)M_a/(M_b + qM_a) \quad (2)$$

$$\varphi_{sb} = 2M_{sb}/(M_b + qM_a) \quad (3)$$

where $M_{segment} = M_b/(q+1)$ is the molecular weight of the segment between two following branching points along the backbone.

In contrast with the traditional coordinate systems for the combs where the dimensionless position along the effective backbone, x_b, is zero at the first branching point,[23−25] here we specify the origin, $x_b = 0$, at the effective backbone's free ends and $x_b = 1$ at the middle of the molecule (Figure 1b). In the traditional approaches, reptation is only considered for the part of the backbone that is not relaxed by fluctuations. Therefore, the outer segments of the backbone, relaxed by fluctuations before reptation time, have no role in the final

reptation process.[23−25] In the TMA model instead, reptation and fluctuations are independent probabilities that are determined for all segments along the backbone and reptation is considered to occur in a tube of effective backbone length.[13,32] Note however that fluctuations will speed up the reptation process through Dynamic Tube Dilution concept (see eq 21), and that the terminal relaxation time of the molecules is determined from the combination of both processes (see eqs 4,5).[36] The dimensionless positions along short and long branches change from zero at the free end of the branches to one at the branching points as depicted in Figure 1.b.

II.2. TMA Model Overview. At times shorter than the characteristic Rouse time of an entanglement, chain dynamics are not affected by topological constraints and are instead governed by fast Rouse modes. At longer times, segments are prevented from lateral motions and the concept of tube becomes relevant. The outermost segments of the backbone and branches start relaxing their orientation by fluctuations, like the arms of a star, while the frozen branching points hold the inner backbone segments oriented. For segments with a potential barrier less than thermal energy ($U < kT$), fluctuations follow the unconstrained Rouse mechanism while deeper segments are slowed down and become activated by the entropic barrier. Since the fluctuation times of deeper segments are exponentially separated, contour length fluctuations can instantaneously take the advantage of extra solvent corresponding to relaxed segments, according to DTD. After complete relaxation of the side branches, the backbone is free to fluctuate in a dilated tube as a linear chain with extra friction blobs at branching points. Finally the effective backbone can reptate in a tube dilated according to the extended Graessley criterion[13] with friction coming from both the relaxed side branches and the monomeric friction of backbone segments.

The relaxation modulus of a monodisperse polymer melt is generally described by three terms representing the relaxation of the polymer from its equilibrium state by reptation or fluctuations ($\mathbf{\Phi}(t)$), constraint release ($\mathbf{\Phi}_{CRR}(t)$), longitudinal Rouse modes and finally the unconstrained fast Rouse motions inside the tube:

$$G(t)/G_N^0 = \Phi(t)\Phi_{CRR}^{\alpha}(t) + F_{Rouse,\,longitudinal}(t) + F_{Rouse,\,fast}(t) \quad (4)$$

where $\Phi(t)$ is the global survival probability from reptation and fluctuations and represents the unrelaxed fraction of the initial tube segments, while $\Phi_{CRR}(t)$ determines the effective tube diameter by taking into account the constraint release Rouse motion (CRR). The survival probability $\Phi(t)$ can be calculated by summing up the contributions from all segments along the chain path that have survived by both reptation and fluctuations relaxation mechanisms:

$$\Phi(t) = \sum_i \varphi_i \int_0^1 (p_{rept}(x_i,t)p_{fluc}(x_i,t))\,\mathrm{d}x_i \quad i\text{: } eb, a, sb \quad (5)$$

where $p_{\mathrm{rept}}(x_i,t)$ and $p_{\mathrm{fluc}}(x_i,t)$ are the probabilities that segment x_i survives from relaxation by reptation and fluctuations, respectively, at time t, and φ_i is the volumetric fraction of part i of the molecule, either the effective backbone (*eb*), branches (*a*) or short branches (*sb*).

According to the TMA model, the characteristic times corresponding to the different relaxation mechanisms are determined based on the unrelaxed polymer fraction at each time step, and the survival probabilities of the segments have to be updated in consequence. In this way the relaxation modulus, $G(t)$, is determined at each time step without using an explicit analytical function. The dynamic storage and loss moduli (G' and G''), can be derived from the relaxation modulus using Schwarzl approximation.[38] In the following sections, different elements of the TMA model used in this overview are explained in detail.

II.3. Branch Fluctuations. Contour length fluctuations are the only possible way for the dangling short and long branches of a comb to relax completely, following the same rules as fluctuations of the arms of a star:[8]

$$p_{fluc}(x,t) = \exp\left(\frac{-t}{\tau_{fluc}(x)}\right) \quad (6)$$

The early fluctuation times for segments with potential barrier less than thermal energy ($U < kT$) follow unconstrained Rouse motions:

$$\tau_{early}(x) = \frac{9\pi^3}{16}\tau_e x^4 Z^4 \quad (7)$$

where $Z = M/M_e$ is the number of entanglements of the branch. For deeper segments, retraction needs to overcome the potential penalty:

$$U(x) = \frac{3kT}{2Nb^2}(L_{eq}x)^2 + \mathrm{const} \quad (8)$$

$$\tau_{late}(x) = \tau_0 \exp\left(\frac{U(x)}{kT}\right) \quad (9)$$

where L_{eq} is the equilibrium length of the branch. Since characteristic fluctuation times of segments along a branch are well separated, we can consider the outer relaxed segments as solvent for the relaxation of inner segments. The first difference with the calculation of fluctuation times of the arms of a star is the presence of the frozen part of the backbone, which is considered in eq 10-2:

$$\frac{\partial[\ln \tau_{late}(x)]}{\partial x} = 3Zx\Phi(x)^{\alpha} \quad (10\text{-}1)$$

$$\Phi(x) = \varphi_{eb}(1-x_b) + \varphi_a(1-x_a) + \varphi_{sb}(1-x_{sb}) \quad (10\text{-}2)$$

The dimensionless positions x_{b}, x_{a}, and x_{sb} correspond to segments of the effective backbone, branches and short branches are related by potential equivalency as described by Milner, McLeish,[40] and Blottiere et al.:[41]

$$x_2 = x_1\sqrt{M_1/M_2} \quad (11)$$

where x_1 and x_2 are the corresponding transition segments on subchains with molecular weight of M_1 and M_2, respectively.

The transition between two fluctuations processes happens at a transition segment x_{trans}, for which the potential is equal to the thermal energy ($U(x_{trans}) = kT$). The TMA model uses a unique expression that guarantees the continuity of the fluctuation times curve at the transition segment:

$$\tau_{fluc}(x) = \tau_{early}(x) \quad \text{for } x < x_trans \quad (12\text{-}1)$$

$$\tau_{fluc}(x) = \tau_{early}(x_{trans})\exp\left(\frac{\Delta U(x_{trans} \rightarrow x)}{kT}\right) \quad \text{for } x > x_{trans} \quad (12\text{-}2)$$

II.4. Backbone Fluctuations. The free ends of the effective backbone fluctuate similarly as the branches of a star molecule as described in section II.3. Before complete relaxation of the short branch, the first branching point is frozen and

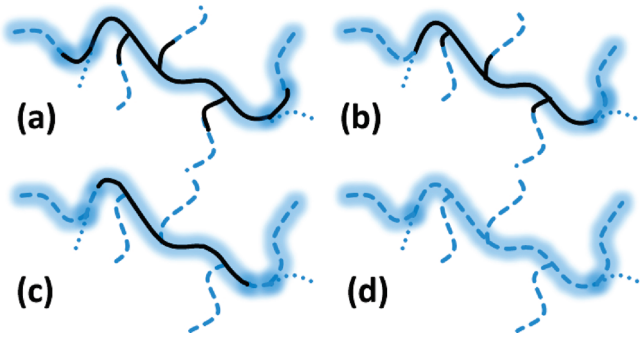

Figure 2. Schematic representation of fluctuations of a comb by triple fluctuations modes (TFM). The effective backbone is highlighted, short branches are represented by dotted curves, relaxed and unrelaxed segments are illustrated by dark bold and bright broken curves, respectively: (a) until the complete relaxation of the short branches, the outer segments of the backbone relax according to the first branching point (mode 1); (b and c) after relaxation of short branches but before long branches are fully relaxed, the outer segments of the backbone can fluctuate (b) first, according to mode 1 or mode 2 (i.e., the second branching point) and (c) then only according to mode 2; (d) after relaxation of long branches, the backbone fluctuates according to mode 3.

the inner segments of the backbone cannot fluctuate. The outermost segments of the free ends can only fluctuate with respect to the first branching point, i.e., they can only fluctuate in "first mode". After complete relaxation of the short branches (see Figure 2a), the remaining oriented segments of the free backbone's ends can also fluctuate with respect to the second branching point, i.e., according to the "second mode". Fluctuations by the first mode (i.e., according to the first branching point) suffer from more potential penalty since the free end has reach deeper fluctuations levels, i.e. to squeeze its length more toward the branching point, but only experience monomeric friction. On the other hand, fluctuations by the second mode suffer from more friction coming from the relaxed short branch but only need shallower fluctuations. So, after relaxation of the short branches, the segments between the relaxed part of the backbone and the first branching point are allowed to fluctuate by either first or second fluctuations modes and we expect that the segments will relax by the faster option. This mechanism corresponds to the transition from Figure 2a to Figure 2b.

Going toward deeper segments along the backbone, there comes a point when relaxation has reached the first branching point but not yet the second branching point. At this stage, the effective backbone can only relax by fluctuations with respect to the second branching point (since the first mode is exhausted and, due to the immobility of branching points of the side- branches, fluctuations with respect to the inner branching points are still impossible). This corresponds to the transition from Figure 2b to Figure 2c. (Note that in the specific case of a comb polymer with few short side-branches (and thus with $M_a = M_{sb}$), this step does not exist, since the short and "normal" side-branches are relaxed simultaneously.)

Later still, after complete relaxation of all the side-branches, all branching points become mobile at once and the backbone can fluctuate in a dilated tube. In most of the former tube models proposed for comb architecture, fluctuations of the backbone exclusively happen with respect to the middle of the molecule.[23−25] In our new model, backbone segments are free to fluctuate with respect to all branching points. Note that a similar idea has been proposed in ref 17 for branch-on-branch structures, without, however, looking at the influence of this statement on the relaxation of the comb polymer. Fluctuations with respect to closer branching points have the advantage of carrying less extra friction from relaxed side branches. On the other hand, fluctuations with respect to the middle of the molecule have the advantage of suffering from less potential penalty. This effect has not been tested yet on comb polymers and we think it could be very important. As will be shown later, fluctuations with respect to the middle of the molecule are favored when the extra friction coming from the side branches is negligible, but fluctuations with respect to the closest branching point are more likely when the relaxed branches provide a drag that outweighs the monomeric friction along the fluctuating part of the backbone. The difference between the predictions with and without considering this effect becomes very significant when stepwise fluctuations are favored due to significant friction of relaxed long side branches. We call this new relaxation possibility the multifluctuations-modes (MFM) relaxation. In this approach, the probabilities of fluctuating with respect to all branching points have to be calculated and the segment is considered relaxing according to the fastest mode. Keeping in mind that the extra friction affects the early time fluctuations through τ_e, we have to adjust the total friction for each fluctuations mode:[13]

$$\xi_{tot} = N_i\xi_0 + \frac{2kT}{a^2}\left(\tau_{fluc,sb}(1) + (i-2)\tau_{fluc,a}(1)\right) \qquad (13)$$

where ξ_0 is the monomeric friction coefficient, the first term on the right side accounts for the drag due to the monomeric friction of the effective backbone segments involved in mode i, and the second term is the contribution from the branches that have to be carried in that mode.

It is more convenient to divide the effective backbone into mobile (*meb*) and immobile (*imeb*) parts as follows:

$$\varphi_{eb}(1-x_b) = \varphi_{imeb} + \varphi_{meb}(1-x_{mb}) \qquad (14)$$

where x_{mb}, the dimensionless position along the mobile part of the effective backbone, changes from zero at the free end of the backbone to one at the frozen branch point at each fluctuation mode. The corresponding volume fractions correspond to the first fluctuation mode are defined as:

$$\varphi_{meb} = 2\max(M_a, M_{segment})/(M_b + qM_a) \qquad (15\text{-}1)$$

$$\varphi_{imeb} = (q-1)M_{segment}/(M_b + qM_a) \qquad (16\text{-}1)$$

Before complete relaxation of the short branch, the first branching point is frozen and the mobile part of the backbone is limited to the free ends of the effective backbone. Therefore, the dimensionless position x_{mb} changes from zero at the free end of the effective backbone to one at the first branching point. After relaxation of the short branch, the first branching point is no longer frozen and the mobile part of the backbone, which corresponds to the next fluctuations mode, will increase by $M_{segment}$ (Figure 2, parts a and b). The dimensionless position x_{mb} now changes from 0 at the free end of the effective backbone to 1 at the second branching point. The remaining oriented part of the outermost backbone segments can therefore feel a new environment where the potential equivalency (eq 11) should now be updated by taking into account the longer mobile part of the effective backbone. As a consequence, when the side-branches are relaxed up to the branching points, the relaxed part of the backbone can be longer than $\max(M_a, M_{segment})$ (Figure 2.c), according to eq 11.

If the backbone can relax by reptation, it will be the final step of the relaxation process. Hence we can neglect the effect of the solvent coming from relaxation by reptation on fluctuation times and late fluctuation times can be calculated according to eqs 7−14, except for the volume fraction of

mobile and immobile parts of the effective backbone that should be updated at each fluctuations mode. It should also be noted that the dimensionless position for fluctuations mode i varies between zero at the free end of the effective backbone to one at the ith branching point:

$$\varphi_{meb} = (2 \quad \max(M_a, M_{segment}) + 2(i-1)M_{segment})/(M_b + qM_a) \tag{15-2}$$

$$\varphi_{imeb} = (q + 1 - 2i)M_{segment}/(M_b + qM_a) \tag{16-2}$$

As a simpler approach to describe fluctuations of the effective backbone after relaxation of all side branches, we can consider that all inner backbone segments only fluctuate with respect to the middle of the molecule. This approach, which involves just three fluctuations modes (with respect to first branching point, second branching point and middle of the molecule), is a simplified MFM approach where all inner backbone segments fluctuate in the last mode. Figure 2d shows the last step of fluctuations according to this triple-fluctuations-modes (TFM) approach.

As discussed by van Ruymbeke et al.[13] for the case of a pom-pom molecule, the transition between two successive fluctuations modes may lead to discontinuity of fluctuation times at the branching points. Indeed, in reality, fluctuation of the backbone chain ends is a superposition of several relaxation modes, from the fast relaxation modes at the chain extremities (which have low friction) to the slower relaxation modes toward the backbone center (which have higher friction). The fast fluctuations of the outer modes are still active when the internal modes become important, and these faster modes contribute to the relaxation of internal tube segments (speeding up their relaxation). Thus, a one-dimensional approximation to the relaxation based on a single internal mode (with friction summed over all side arms, and fluctuation coordinate x set to zero at the chain end) will overestimate the relaxation time. In order to account for this, we rescale the relaxation coordinate x so that the point $x = 0$ from which the retraction potential is calculated no longer corresponds to the chain end (but, rather, is a point internal to the backbone chain). For each mode, we fix the point $x = 0$ by requiring continuity of relaxation times across the branching points, rescaling the outer part of the effective backbone, between the free end and the last branching point at $\max(M_a, M_{segment})+(i-2)M_{segment}$. In such a way, the fluctuation time of the segment right before the $(i-1)$th branching point in mode $i-1$, is equal to the fluctuation time of the segment right after that branching point, in mode i:[13]

$$\tau^{i}_{fluc}(x_{br.point}) = \tau^{i-1}_{fluc}(1) \tag{17}$$

$$x_{br.point} = \frac{M_n}{M_n + M_{segment}} \tag{18}$$

where M_n is the rescaled length of the outer part of the backbone in mode i. In other words, the length of the mobile part of the equivalent backbone would be $M_n+M_{segment}$. Therefore, it takes a time equal to $\tau_{fluc}{}^{i-1}(1)$ for the free end of the effective backbone of the equivalent comb molecule to diffuse up to the last branching point in mode i, while feeling the total friction according to eq 13, as explained in details in ref 13. In this new coordinate system, the dimensionless position $x_{b,rescaled}$ varies from zero at the free end of the rescaled effective backbone to one at ith branching point.

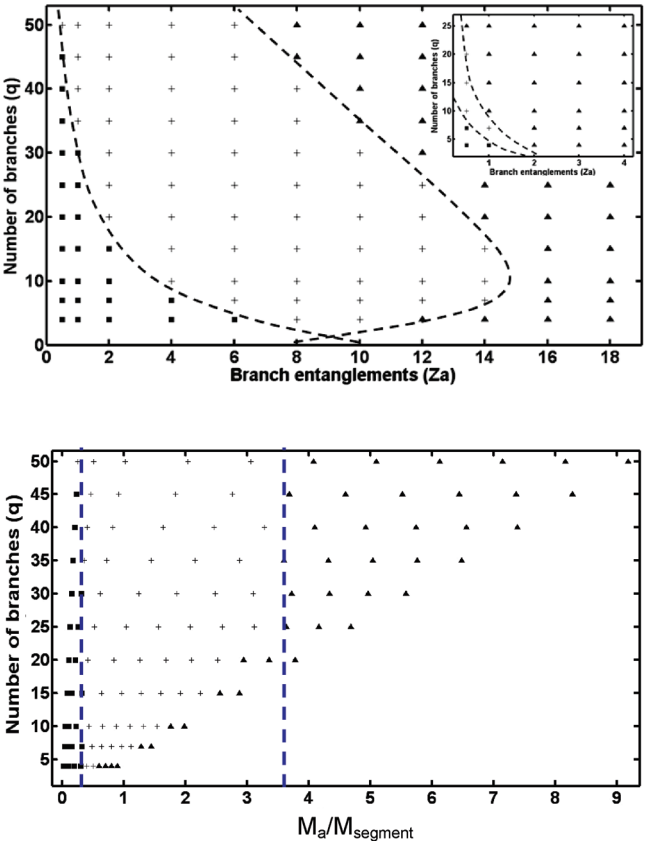

Figure 3. Contour plot of fluctuations behavior of combs with 100 and 20 (inset) numbers of backbone entanglements as a function of (a) the number of branch entanglements or (b) the ratio between M_a and $M_{segment}$: linear-like fluctuations, where there is no rescaling (squares), intermediate zone, where the number of rescaling is less than the number of modes (crosses), and fully hierarchical fluctuations, where the number of rescaling is equal to the number of modes (triangles). Lines are for guiding the eye.

For calculating the corresponding fluctuation times in the rescaled coordinate, x_b should be replaced by $x_{b,rescaled}$:

$$x_{b,rescaled} = [x_b(\max(M_a, M_{segment}) + (i-1)M_{segment}) - (i-2)M_{segment} + M_n - \max(M_a, M_{segment})]/[M_n + M_{segment}] \tag{19}$$

In this way, a continuous fluctuation times curve can be obtained for both the MFM and TFM approaches.

Superiority of the stepwise hierarchical fluctuations idea, as considered in MFM approach, versus the simple picture of fluctuations with respect to the middle of the molecule, as assumed in former tube models for combs, depends on the detailed structure of the comb. There are a lot of structural variations possible for combs, leading to numerous classes of relaxation behavior and it is therefore a complex task to carry out a systematic sensitivity analysis for the dynamic behavior of combs as a function of structural variables. Here, we consider a limited set, corresponding to the range covered by the experimental data tested in this paper. Thus, we analyze the fluctuations of two series of combs, with 100 and 20 backbone entanglements, respectively. Figure 3 presents a contour plot of the regions characterized by linear-like, intermediate, and hierarchical behavior, as a function of number and length of branches, or as a function of the ratio between M_a and $M_{segment}$. There is a zone where combs fluctuate with respect to the middle of the molecule, at low

branch entanglement levels and low number of branches. Opposite, there is a zone where comb segments fluctuate with respect to the closest branching point, at high number of branches and high level of branch entanglements. In between, there is an intermediate region where outer backbone segments fluctuate with respect to the closest branching points and inner segments fluctuate with respect to the middle of the molecule. When plotted as a function of the ratio $M_a/M_{segment}$ (see Figure 3b), we observe an almost vertical transition between linear like fluctuations and the intermediate zone (around $M_a/M_{segment} = 0.4$). For combs with a large amount a branches ($q > 25$), a second transition appears around $M_a/M_{segment} = 3.5$, separating the intermediate region and the fully hierarchical fluctuations.

Figure 3 highlights the finding that the linear like behavior is limited to a narrow range of comb structures and for most combs, partial to fully hierarchical fluctuations are the rule. In this case, a MFM approach is superior. Note that the BoB model[17] also considers different fluctuation modes, but in a different way than the one proposed here. In this model,[17] the contributions from the different branching points to the final fluctuation times of the backbone segments are considered separately rather than summing up their contributions as proposed in eq 13.

II.5. Backbone Reptation. The probability of relaxation by reptation at time t, for a segment of the effective backbone at position x, is calculated by the classical Doi−Edwards equation:[2]

$$p_{rept}(x,t) = \sum_{i,\,odd} \frac{4}{i\pi} \sin\left(\frac{i\pi x}{2}\right) \exp\left(\frac{-i^2 t}{\tau_{rept}}\right) \qquad (20)$$

The characteristic reptation time of a comb molecule is calculated by taking into account the contribution of the monomeric friction of the backbone segments and the extra friction coming from relaxed side branches, to the total drag:[11,13]

$$\tau_{rept} = 3\tau_e Z^3 \Phi^{\alpha}_{active}(t) + \frac{2}{\pi^2} Z^2 (2\tau_{fluc,\,sb}(1) + (q-2)\tau_{fluc,\,a}(1)) \Phi^{2\alpha}_{active}(t) \qquad (21)$$

where the first term represents the contribution of monomeric friction of the effective backbone segments and the second term corresponds to the contribution of relaxed short and long branches. If the characteristic times of fluctuations and reptation mechanisms were well separated, the reptation process can take the advantage of the fluctuations solvent and the backbone reptates in a fully dilated tube. Although, as the global effect of constraint release, the tube can dilate gradually by CRR motions, it also takes a while for the linear backbone to fill the dilated tube by lateral Rouse motions. In other words, the fast relaxing parts can be considered as solvent for relaxation of slow relaxing parts only if the oriented fraction has enough time to explore the dilated tube, which itself dilates at rate controlled by CRR process. Since fluctuation times of successive segments are exponentially separated, the relaxed parts have enough time to act as solvent for the fluctuations of oriented segments, and therefore DTD works. The problem arises when one has a system with different relaxation times that might be not well separated. This can be the case for complex architecture (including combs) or blends of different structures.[42−46] In the TMA model the rate at which the linear chain can take the advantage of the solvent is determined by the so-called extended Graessley criterion:[13]

$$\Phi_{active}(t) = \Phi(t/Z^2) \qquad (22)$$

In a classical case of binary blends of two monodisperse linear chains with widely separated molecular weights, after reptation of the short chains, it takes a time equal to $\tau_{dS} Z_L^2$ for the long chain to occupy the effective tube diameter. So if a solvent appears at time τ_{dS}, it takes $\tau_{dS} Z_L^2$ to be felt.[5] Conversely, for a chain to benefit from new solvent at time t, that solvent has to appear at time t/Z^2. The TMA model allows looking back through time space and updating the active solvent at each time step. The lag time between global survival probability and the "active solvents", i.e. the solvent truly effective in dilating the tube, guarantees the time required for the chain to fill the dilated tube by Rouse like lateral movements. Therefore, the reptation time is not a constant value and it evolves through time, parallel to the unrelaxed polymer fraction. The global effect of CRR process is to limit the maximum rate at which the entanglement density can decrease:

$$\Phi_{CRR}(t_i) \geq \Phi(t_{i-1}) \left(\frac{t_{i-1}}{t_i}\right)^{0.5} \qquad (23)$$

II.6. High Frequency Rouse Relaxation. The second and third terms of eq 4 are the longitudinal relaxation modes and fast Rouse motions inside the tube, which can be calculated as:

$$F_{Rouse,\,longitudinal}(t) = \sum_i \frac{\varphi_i}{4Z_i} \sum_{j=1}^{Z_i - 1} \exp\left(\frac{-j^2 t}{\tau_{Rouse,\,i}}\right) \quad i: eb, a, sb \qquad (24)$$

$$F_{Rouse,\,fast}(t) = \sum_i \frac{5\varphi_i}{4Z_i} \sum_{j=Z_i}^{N} \exp\left(\frac{-2j^2 t}{\tau_{Rouse,\,i}}\right) \quad i: eb, a, sb \qquad (25)$$

where N is the number of Kuhn segments and $\tau_{Rouse,i} = \tau_e Z_i^2$ is the Rouse time for different parts of the comb including the effective backbone and normal and short side branches.

II.7. Modification of Early Time Fluctuations. Recently, van Ruymbeke et al. have investigated the origin of discrepancies between measured values of plateau modulus and predictions from traditional tube models.[36] For poorly entangled chains, tube models predict that the storage modulus at a frequency equal to the inverse of Rouse time of an entanglement, $1/\tau_e$, is strongly molecular weight dependent.[47−50] Since at this time the entanglement obstacles cannot be felt, the equilibrium values should not depend on molecular weight. By investigating the fluctuation times of a moderately entangled linear polymer, they have noticed that a significant portion of the chains is predicted to relax before τ_e, which is inconsistent; i.e., a considerable fraction of polymer has relaxed from its equilibrium state, before even reaching to this state by longitudinal and fast Rouse motions. The problem arises because tube models usually consider relaxation by reptation or fluctuations to start immediately after deformation. In reality, the chain needs the characteristic Rouse time of an entanglement, in order to restore the equilibrium in the tube. Missing this point leads to underestimation of early fluctuation times of the chain. To overcome this problem van Ruymbeke et al. have proposed a rescaled segmental coordinate system, so that the predicted

fluctuation time at $x = 0$ is equal to τ_e:

$$\tau_{fluc}(x = 0) = \tau_{fluc}\left(x_{rescaled} = \frac{M^+}{M + M^+}\right) = \tau_e \quad (26)$$

where M^+ is the molecular weight of the segment added to the chain ends (close to half M_e), and M is half the molecular weight of a linear chain or the molecular weight of a branch.

For using the calculations in this new coordinate system, the dimensionless position along the actual chain, x, should be rescaled as follows:

$$x_{rescaled} = \frac{xM + M^+}{M + M^+} \quad (27)$$

The improvement for long chains will be negligible, but this correction becomes very important for weakly entangled chains. In particular, in the case of combs with a large number of small side branches, this modification is expected to play a significant role.

III. Results and Discussion

III.1. Materials and Parameters. In order to evaluate the capability of the TMA model to predict LVE properties of different classes of comb architectures, independent from their chemistry, the model was applied to experimentally available data from three references.[25,28,29] Molecular characteristics of all low polydispersity anionic samples used in this work are described in Table 1. The first samples consist of two series of PS combs named c6 and c7, comprising linear backbones of 275 and 860 kg/mol, respectively, and approximately $q = 25-30$ side branches of molecular weight increasing from 6.5 to 98 kg/mol, i.e., from almost half an entanglement up to six entanglements. The chemistry dependent parameters τ_e, M_e, and G_N^0 were respectively fixed to 0.6 to 1×10^{-3} s, 14 kg/mol, and 0.24 MPa at the reference temperature of 170 °C. Note that τ_e slightly depends on the samples architecture. This is not unreasonable as τ_e reflects the local dynamics, through monomeric friction and hence depends on the chemical structure (and of course temperature) as explained by Liu et al.[46] Such a structure dependence of τ_e has been previously reported in literature.[25] The next samples are three PBd combs consisting of 50 kg/mol linear backbone and including $q = 17-18$ side branches of various molecular weights between 7 and 23.2 kg/mol, which implies both backbone and branches are well-entangled. The corresponding material parameters are $\tau_e = 1$ to 1.5×10^{-6} s, $M_e = 1.65$ kg/mol, and $G_N^0 = 1.1$ MPa at reference temperature of 27.5 °C. These samples were synthesized by Roovers[37,39] and recently remeasured by Kapnistos et al.[25]

The next set of data consists of two series of PI combs, synthesized by Hadjichristidis and used by Kirkwood et al.[28] and Lee et al.[29] respectively. Altogether, those samples consist of linear backbones with molecular weights varying from 85 to 370 kg/mol and approximately $q = 4-18$ branches with molecular weights between 2.7 to 17.9 g/mol, i.e. from almost half an entanglement to about four entanglements. The corresponding material parameters used in this work are $\tau_e = 6 \times 10^{-6}$ s, $M_e = 3.9$ kg/mol, and $G_N^0 = 0.55$ MPa at reference temperature of 25 °C.

For all three polymers, the M_e vs G_N^0 relationship almost perfectly follows the "G" definition according to ref 51 and is in good agreement with previously reported values by Kapnistos et al.,[25] Liu et al.,[52] and Fetters et al.[53]

We use the value $\alpha = 1$ for the dilution exponent, consistently with our previous works.[13−17,46] Kapnistos et al. have found better predictions for combs with linear and star backbones in linear and nonlinear regimes using this value.[25,26,54] They have also shown that despite of using $\alpha = 1$, their model predictions for the ratio between the plateau modulus before and after relaxation of branches has the correct scaling with respect to the backbone volume fraction (approximate power 7/3).[25] As mentioned before, we have avoided the use of an adjustable branch point hopping fraction parameter p^2 by fixing its value to 1.

Table 1. Molecular Characteristics of the Combs Used

sample	$M_{backbone}$ (kg/mol)	M_a (kg/mol)	q (branches/backbone)	ref
PS-c712	860	6.5	31	25
PS-c722	860	11.7	30	25
PS-c732	860	25.7	25	25
PS-c742	860	47	29	25
PS-c752	860	98	29	25
PS-c612	275	6.5	30	25
PS-c622	275	11.7	28	25
PS-c632	275	25.7	26	25
PS-c642	275	47	29	25
PS-c652	275	98	28	25
PBd-lc1	50	11.3	18	25
PBd-lc2	50	23.2	17.8	25
PBd-lc3	50	7	17	25
PI-132k	85.1	10.2	4.6	28
PI-159k	137	2.7	8.2	28
PI-211k	157	6.3	8.6	28
PI-472k	370	5.8	17.6	28
PI−C14	151	17.9	5	29
PI−C15	90	9.2	4	29

III.2. General Relaxation Behavior of Comb Structures. Figure 4 compares the experimental dynamic moduli of some PS comb samples with longer backbone and various branch lengths, with the corresponding TMA model predictions. The depth of valley in the loss modulus at high frequencies corresponding to the dissipation due to fluctuations of the branches increases with increasing branch length, which is relatively well captured by the model predictions, taken into account the fact that the samples are considered monodisperse both in molecular weight and in architecture (which leads to a too strong and too narrow relaxation peak).[15] In particular, TMA works well for both combs with long and short side branches. Note that there are different elements that might be responsible for this improvement. The most straightforward explanation is that, as the length of side branches decreases (at the same total number of branches) the contribution to the total drag on the backbone from the relaxed branches becomes comparable with the monomeric friction from the backbone segments. Ignoring contribution of monomeric friction in such case would cause the prediction to diverge from the experimental behavior. Predictions made by ignoring monomeric friction of backbone segments are shown by dashed lines in Figure 4. This oversimplification leads to underestimation of the moduli, especially at low frequencies which correspond to the backbone terminal relaxation. However, it leaves intermediate frequencies, corresponding to the relaxation of branches, totally unchanged. Influence of monomeric friction of backbone segments becomes more pronounced as the length of branches decreases (also consider Figure 4b for sample PS-c712 with the shortest branches for this set of combs). Note that the predicted backbone reptation peaks are narrower and higher than the experimental features. This discrepancy is believed to be due to ignorance of samples polydispersity.[13,25] As explained by van Ruymbeke et al.[13] polydispersity smears out the relaxation peak. Because of the large influence of branch length on the motion of branching points and reptation of the backbone, dispersity of branch length

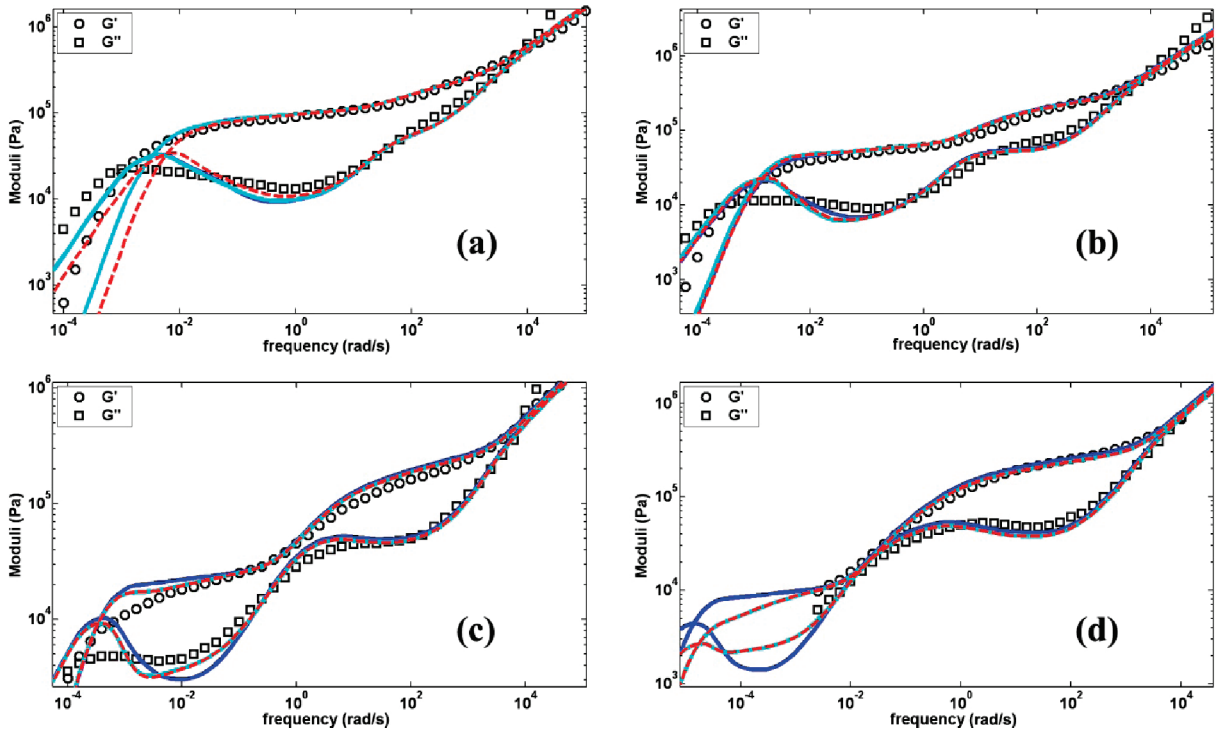

Figure 4. Experimental dynamic moduli (points) and TMA model predictions; MFM approach (bright lines), TFM approach (dark lines) or MFM approach without accounting for the monomeric friction of backbone segments (dashed lines), for PS-c7 comb samples: (a) PS-c722, (b) PS-c732, (c) PS-c742, and (d) PS-c752. Note that in part a, results obtained by considering the TFM approach or the MFM approach superimpose.

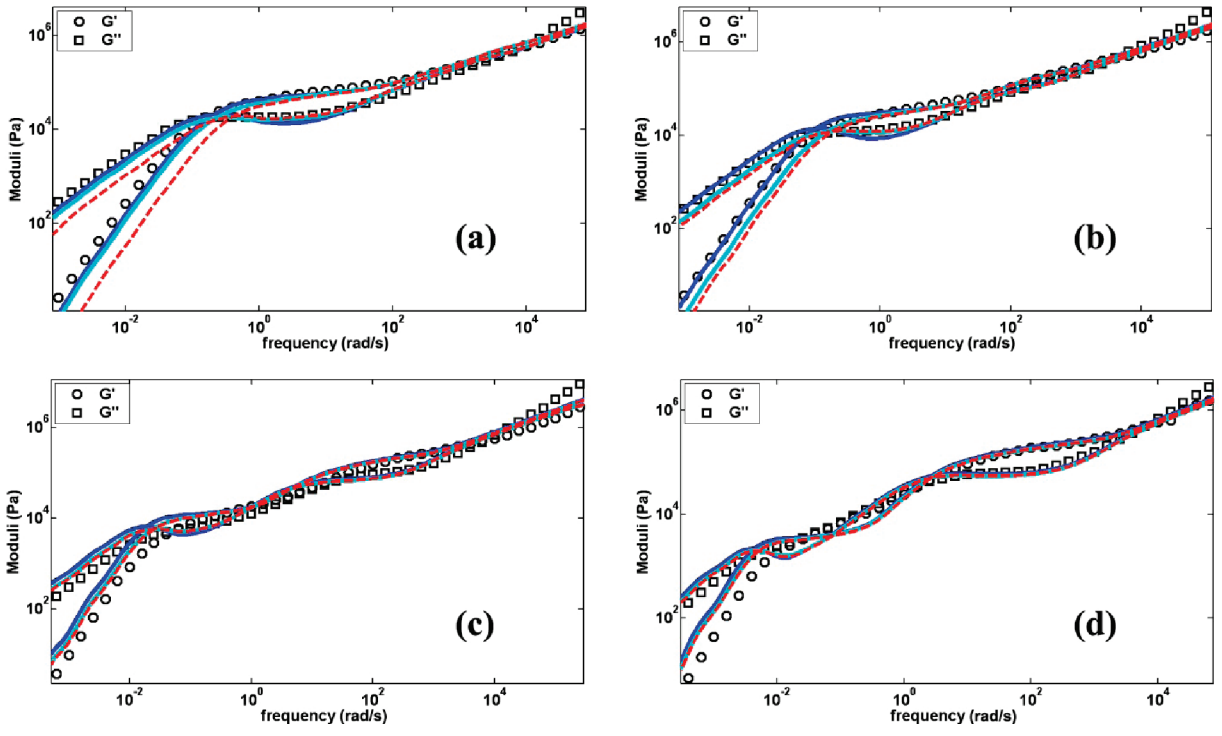

Figure 5. Experimental dynamic moduli (points) and TMA model predictions; MFM approach (bright lines), TFM approach (dark lines), or MFM approach without accounting for the monomeric friction of backbone segments (dashed lines) for PS-c6 comb samples: (a) PS-c612, (b) PS-c622, (c) PS-c632, and (d) PS-c642.

has a very significant effect. The effects of polydispersity will be discussed later in section III.4.

Figure 5 compares the experimental behavior of some selected PS comb samples with shorter backbone and various branch lengths, with the corresponding TMA model predictions. Again the model predictions properly capture the behavior of both combs with short and long branches. As the friction barrier due to the relaxed branches increases (due to increase of the branch lengths) the MFM predictions become superior as can also be seen in Figure 6d for sample PS-c652 having

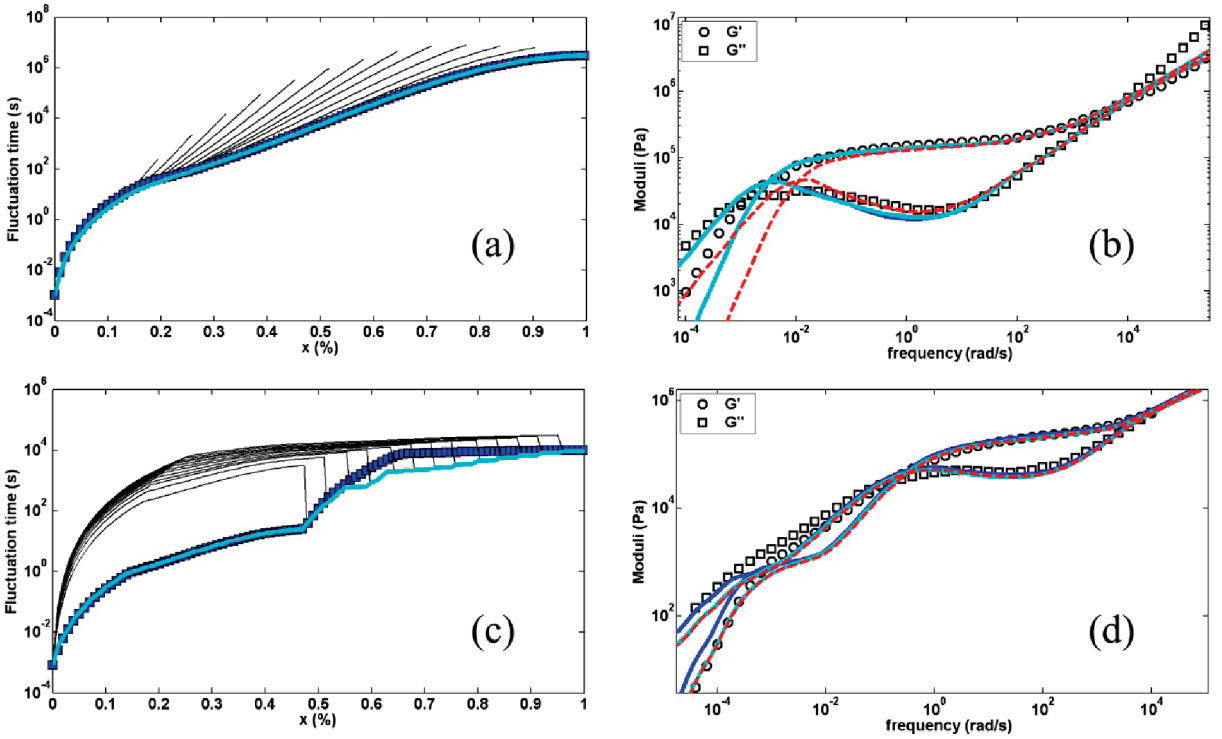

Figure 6. Fluctuation times of the effective backbone; different fluctuations modes (thin lines), MFM approach (bright lines), TFM approach (squares) [(a) PS-c712, (c) PS-c652] and corresponding LVE predictions [(b) PS-c712, (d) PS-c652], by considering the MFM approach (bright lines), the TFM approach (dark lines), or the MFM approach without considering the monomeric friction of backbone segments (dashed lines). Note that in part b, results obtained by MFM and TFM superimpose.

longest branches for this set. This is due to the fact that, when the backbone segment between two following branches becomes shorter and the length of side branches increases, the friction from relaxed branches outweighs the potential barrier and the segment prefers to retract toward closer branching points instead retracting with respect to ones farther, thus avoiding the price of carrying the friction of the relaxed branches. In other words, in the extreme case when the extra friction from side branches is very high, fluctuations take place step by step, just as in a Cayley-tree molecule where inner generations wait for the relaxation of outer generations. In the long-branch comb case, the inner backbone segments wait for full relaxation of outer segments of the backbone to start their fluctuations.[15,16] Considering a Cayley-tree-like behavior, the MFM approach provides the most precise predictions. On the other hand, when the side branches are so short that their contribution to the total friction becomes imperceptible, the backbone prefers to carry all the relaxed branches and take the advantage of a smaller potential barrier by fluctuating with respect to the middle of the molecule. In this extreme case where the comb simulates a linear chain behavior, the more simple TFM approach provides the same precise predictions as MFM, and due to lower calculation costs, it will be preferred. This ensures consistency of the model, which stays valid for extreme structures. Predictions obtained by ignoring the contribution of monomeric friction of backbone segments are again shown by dashed lines in Figure 5. In comparison to Figure 4, it is clear that the significance of monomeric friction is reduced for combs with shorter backbones.

Figure 6 shows model predictions and the corresponding backbone fluctuation times for two extreme cases of PS combs, already mentioned above. In sample PS-c712, the side branches are half an entanglement long and the length of backbone segments between branches is considerable. Hence, the potential barrier for retraction along the backbone is high and dominates the extra friction from short side branches. Figure 6a shows the corresponding relaxation times for all possible fluctuations modes as well as selected fluctuation times according to TFM and MFM approaches. In this specific case, the backbone segments relax faster with respect to the middle of the molecule than with respect to the next branching point. Therefore, the result of the MFM approach, which always considers the faster mode, is identical to the TFM approach, and no switch from one mode to another one is observed. Thus, for these short branches, segments prefer to fluctuate like a linear chain, with respect to the middle of the molecule, as this corresponds to the lowest potential barrier. Fluctuation times according to MFM merge with the predictions of TFM as extra friction from relaxed branches become negligible. Conversely, in sample PS-c652, side branches are longer than six entanglements and the backbone is shorter which implies exponentially higher extra friction and lower potential barrier at each mode. Figure 6c shows the corresponding backbone fluctuation times. Now, segments relax by fluctuations with respect to the closest branching point, which requires a rescaling of the outer part of the backbone in order to keep the continuity of the fluctuation times curve (see section II.4). In this case, fluctuations according to MFM are faster than according to TFM and the corresponding predictions of dynamic moduli are in better agreement. All PS combs of the c6 series with shorter backbones behave like Cayley-tree molecules and the importance of using MFM increases in relation to branch length. While sample PS-c712 thoroughly fluctuates like a linear chain, sample PS-C752 exhibits a pure Cayley-tree-like behavior. Some polymers like combs of the c7 series relax according to both mechanisms i.e. like a Cayley-tree molecule at the outer segments and like a linear chain at the inner parts of the backbone. Predictions of the model, ignoring contribution of

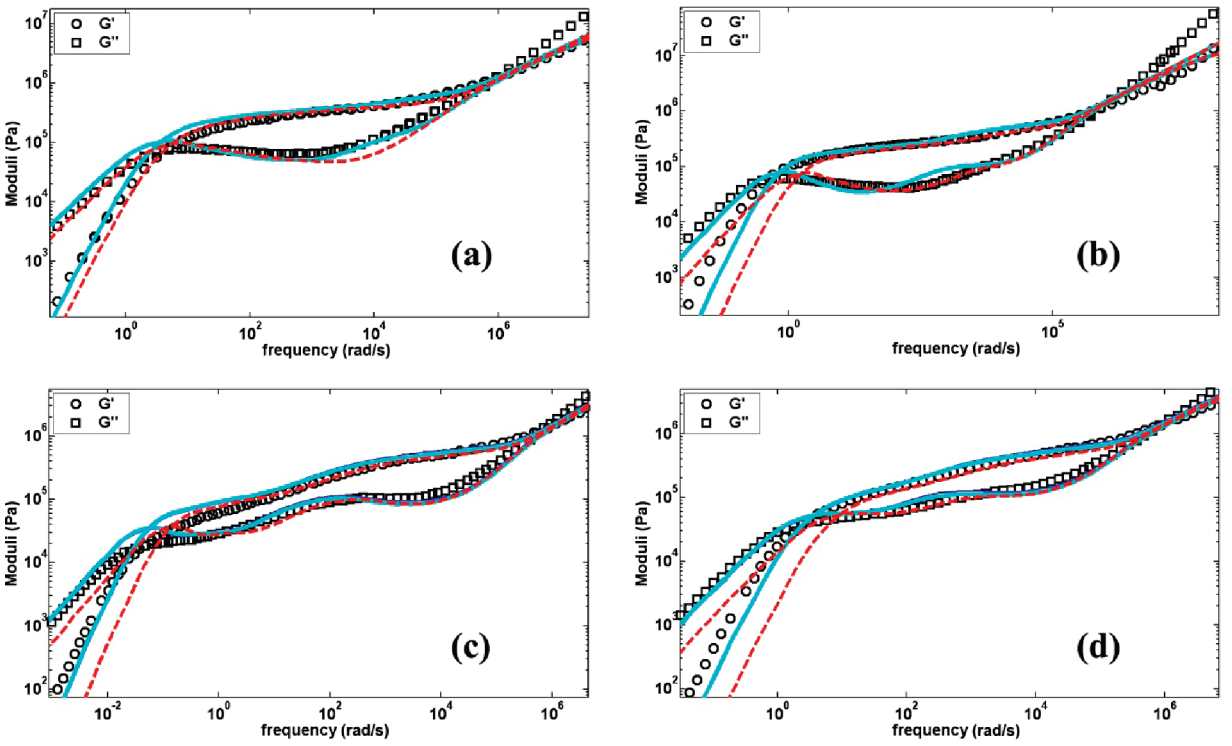

Figure 7. Experimental dynamic moduli (points) and TMA model predictions (lines); TFM approach (dark lines), MFM approach (bright lines), and without modification of early fluctuations (dashed lines), for PI comb samples: (a) PI-159, (b) PI-211, (c) PI-c14, and (d) PI-c15.

monomeric friction are shown by dashed lines, as well. It is apparent that while for combs with long branches, the contribution of monomeric friction to the total drag is negligible, it plays an important role for combs with short branches.

III.3. TMA Model and Extra Drag of Short Side Branches. Recently Kirkwood et al.[28] have used the tube model for combs from the work of Kapnistos et al.[25] in order to see whether it can predict the relaxation of PI combs with unentangled to marginally entangled branches. They found that the model considerably underpredicts the relaxation behavior of combs with shorter branches, leading to the idea that short branches cause more drag than what is expected from tube theories. A recent atomistic simulation by Zhou and Larson on asymmetric stars also suggests a stronger friction from short arms than anticipated.[30] The authors have suggested that the entanglement molecular weight on the time scale of τ_e is roughly half of M_e calculated from the plateau modulus, and this is why the short branches appear to be more effectively entangled. Starting from this proposal, Kirkwood et al. have amplified the corresponding friction by increasing the number of entanglements of side branches so that the model provides correct predictions. However, it can be argued that ignoring the contribution of monomeric friction to the total drag is one of the main missing points in existing models for combs and that it can cause such an underestimation. Nonetheless, neglect of monomeric friction cannot be the full origin of the anomalous drag from short branches, as the problem is still observed in systems that do not suffer from this oversimplification. Frischknecht et al.[11] have extended the original tube model of Milner and McLeish[8] to the case of asymmetric stars by considering the short arm causing extra drag that decreases the curvilinear diffusion rate of the linear backbone formed by the two long arms. The total drag on the reptating backbone is correctly obtained by adding the effective drag caused by the short arm to the drag from monomeric friction along the backbone. Nevertheless, the authors also find that progressively smaller values of p^2 are needed to capture the terminal relaxation behavior of asymmetric stars with lightly entangled branches, confirming that the short arm imposes a larger drag than expected. Recently, Zamponi et al. have used neutron spin echo spectroscopy to compare the motion of labeled branch points of two symmetric and asymmetric polyethylene stars, at the molecular scale.[31] They found that, although the applied tube model predicts that the branching point of the asymmetric star should be able to move along the tube formed by two long arms in the time frame of the observation, a short arm of only one entanglement length is sufficient to localize the branching point, similar to the case of a much longer arm in a symmetric star. This discrepancy between tube models and observed behavior of asymmetric stars should be even more pronounced in the case of combs with short branches. With this question in mind, we have applied the TMA model to available PI combs with unentangled to well entangled branches from different sources.[28,29]

Figure 7 shows the TMA model predictions for some selected PI combs from recent works of Kirkwood et al.[28] and Lee et al.[29] It is interesting that the model can capture the behavior of combs from different sources with the same chemistry dependent parameters. For combs with branches having more than two entanglements, the general behavior is Cayley-tree-like while for the other samples with unentangled to marginally entangled side branches the behavior varies from Cayley tree-like at the outer parts to linear chain-like at the most inner parts. There is no indication of anomalously high friction for the sample with the shortest branches of 2.7 kg/mol molecular weight (Figure 7a). The correct prediction by the TMA model for short branch combs with a standard value for side branch friction is partially due to inclusion of the monomeric friction of backbone segments in the model, but presumably also to the modification of early time fluctuations presented in section II.7. Rescaling of the coordinate system by addition of molecular weight of M^+ to the branches free ends, in order to have fluctuation time τ_e at the branch ends, definitely increases the

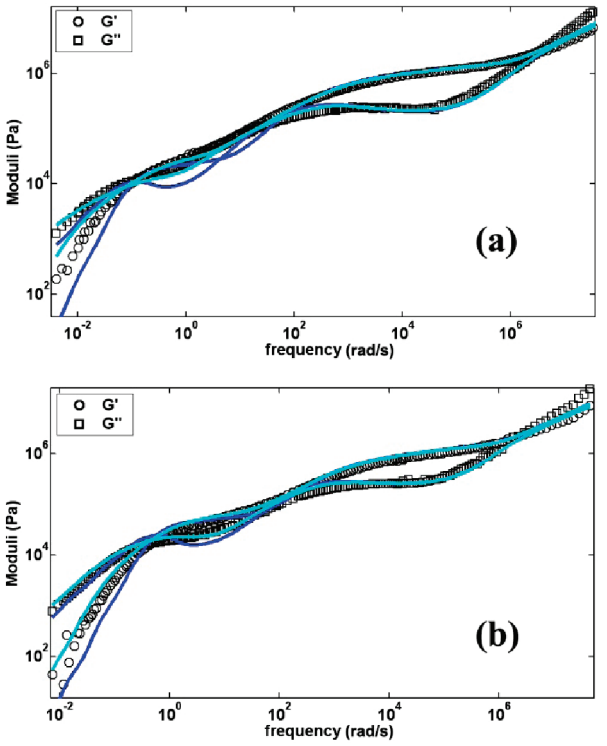

Figure 8. Experimental dynamic moduli (points) and TMA model predictions; MFM approach with (bright lines) and without (dark lines) incorporation of polydispersity effects; for PBd comb samples: (a) PBd-lc1; (b) PBd-lc3.

corresponding friction from relaxed side branches. The behavior of samples in absence of this modification was determined and the corresponding predictions are shown in Figure 7 by dashed lines. In contrast to the contribution of monomeric friction, it can be noticed that the early fluctuation time modification also affects the intermediate zone corresponding to the relaxation of side branches. It seems that this modification yields a remarkable improvement and is necessary for capturing the general behavior of all samples. As a consequence we can say that ignoring the required time to restore equilibrium in the tube before the start of relaxation mechanisms, as is the case in traditional tube models, can lead to the underestimation of the relaxation time of short branches and impose an artificial extra drag correction.

III.4. Effect of Polydispersity. Figure 8 shows the LVE properties of two of PBd combs with well-entangled branches and corresponding predictions. All samples studied here were anionically synthesized but although polydispersity is low, it can have a large influence on the relaxation spectrum, especially the distribution in length and number of side branches.[25] Moreover, most of commercial polymers are polydisperse and it is very important to incorporate this effect in the study of real polymers.[46] In order to handle polydispersity effect, an approach was introduced by Larson[18] for general branched structures and developed by Das et al.[17] to branch on branch polymers, where at each time step the relaxing segments of all model chains involved are determined.[17−19,21] Besides this method, two indirect ways of incorporating polydispersity have been utilized in literature. Kapnistos et al.[25] have used a simple weighted summation for incorporating different comb structures with each being treated independently. This method has the drawback of ignoring the mutual interaction of chains, which is very important for calculating dynamic dilution. Frischknecht et al. have adjusted the average arm relaxation time with respect to a Gaussian distribution of arm lengths.[11] Daniels et al.[23] and Inkson et al.[24] have also followed the same approach and used modified versions of this treatment. We believe both methods oversimplify the cooperative effect of chain dilution. However, in order to show the influence of polydispersity on the delay of the terminal zone and the broadening of the reptation hump, as a rough estimate, we follow the Kapnistos et al.'s approach. Three backbone lengths, M_b, three branch lengths, M_a, and three number of branches, q, are considered, so that each one is the representative of one-third of a Gaussian distribution.[13] The polydispersity indices of 1.1, 1.1, and 1.05 (as a reasonable "guesstimate" in the absence of experimental values) are used for the backbone length, branch length, and the number of branches, respectively. The overall behavior is calculated by averaging over 27 chains of different structural parameters and the results are shown as bright lines in Figure 8. Polydispersity broadens the spectrum of relaxation times with a shift of the mean value to higher times, which results in "smoothing out" terminal relaxation. The assumptions of random distribution of arms and of a fixed number of arms per comb have been already studied by Chambon et al. and it was shown that this simple analytical approach based on constant number of arms is valid.[27]

Note that, besides the polydispersity in molecular weight, architectural polydispersity (such as small variations in the number of branches per backbone, or in the branches distribution along the backbone) can also influence the linear viscoelastic of comb polymers, which is not discussed in this work.

III.5. Limitation of the Dynamic Tube Dilution concept. It is worth noting that the predictions of the TMA model for the polydisperse sample are very satisfactory and are obtained using $p^2 = 1$ and without manual determination of the extent of tube dilation. In fact there is a strong debate on applicability of DTD in cases where there is a second relaxation process that can take the advantage of solvent coming from the first process.[45,47] There is clear evidence in literature of DTD failure in the case of star and linear chain blends.[42−44] In the case of complex architectures where there might not be enough time separation between relaxation processes that follow each other in the framework of hierarchical relaxation, the same breakdown is suspected. Frischknecht et al. have analyzed the situation for the case of asymmetric stars.[11] They could capture the relaxation behavior by assuming that backbone reptation takes place in the dilated tube and branch point hopping in the "skinny" one (as the undilated tube is sometimes called). By the use of progressively lower p^2 parameter, they could also make good predictions assuming reptation and hopping both happening in the dilated tube. Former models for comb architectures have also proposed the relaxation of backbone to happen in the dilated tube.[23−25] However, since there is no independent evidence for the validity of this assumption and it is not clear whether reptation and fluctuations of the backbone happen in the same dilated tube, we prefer considering here the time evolving solvent described in ref 13, which is based on an extended Graessley condition for determining the tube dilation level. The latter evolves through time from a skinny to a dilated tube. In the model, this is implemented through Φ_{active}, the oriented part of the polymer while $(1 - \Phi_{active})$ is responsible for tube dilation as a function of time. Its evolution is shown in Figure 9, for samples PS-c612 and PS-c652. As it can be seen there is a time lag between creation and effectiveness of the solvent, which guarantees the necessary time for the chain to fill the dilated tube by lateral movements, while the tube itself dilates by CRR process as shown by the dashed lines. Note that for the sample with long branches (see Figure 9b), there is also a lag time for the tube to take the advantage of the disoriented

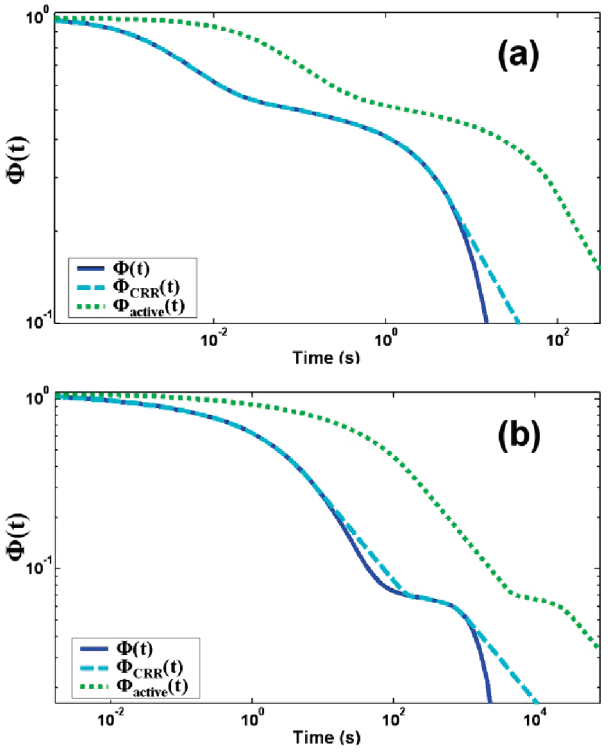

Figure 9. Survival probability (dark lines), contribution of CRR process (dashed lines), and Φ_{active} (dotted lines) for samples (a) PS-c612 and (b) PS-c652.

fraction of the sample and to dilate according to CRR, after relaxation of the side branches.

IV. Conclusions

Although the TMA model is based on the same mesoscopic physics as other tube-based models, the algorithmic implementation of the relevant physical processes is specific. In particular, the expressions for reptation time (eq 21), modified early fluctuation times (eq 26), tube dilation (eq 22), and the method for calculating the overall oriented fraction of polymer (eq 5) are different from former models for comb architectures. In the TMA model, there is neither time scale separation between different relaxation processes nor the flexibility for ad hoc determination of tube dilation effectiveness since it derives from the modified Graessley criterion (eq 22). These features make the TMA model very flexible and highly suited to explore the dynamics of comb structures with widely different characteristics. We have first extended the model to make it suitable for comb architectures. In particular we have introduced the concepts of "Multiple Fluctuations Modes" (MFM) and the simplified version "Triple Fluctuations Modes" (TFM) to cover the wide dynamic range exhibited by combs depending on their branch length. We have also included the early fluctuation times correction recently proposed for linear chains. Next, the extended model was tested on comb samples from several sources and different chemistries, encompassing a broad range of backbone and branch lengths. In all cases, the predictions are found in good agreement with experimental data. In particular, while other tube models require an ad hoc increase of the equivalent friction coming from relaxed branches in order to correctly describe the linear viscoelastic response of short side branch combs,[25,28,30,31] no adjustment of the friction is needed here. This is mainly due to two reasons: the importance of considering the contribution of the monomeric friction from the backbone itself to the total drag, and the importance of considering the time required to equilibrate an entanglement segment before the molecule can start relaxing.[36] Finally, we have studied the extreme limits of relaxation behavior by comb structures with the help of the MFM and TFM approaches. In particular, if the extra friction from the relaxed side branches is significant, comb molecules fluctuate in the same way as a Cayley-tree molecule, i.e., allowing gradually deeper backbone segments to move with respect to the next branching point, from the outer one to the middle one. On the other hand, if the extra friction from the relaxed side branches becomes negligible in comparison with the potential barrier of retraction along the backbone, the whole backbone segments fluctuate just as a linear chain, i.e., with respect to the middle of the molecule.

Acknowledgment. The authors thank Michalis Kapnistos, Keith M. Kirkwood, and Dimitris Vlassopoulos for providing parts of the experimental data and for their useful comments. Financial support by EU under the framework of the DYNACOP project and the SOFTCOMP network is gratefully acknowledged. E.V.R. thanks the Belgian National Fund for Scientific Research (FNRS) for financial support (as Chargé de Recherches). The authors would also like to thank the reviewers for their constructive comments.

References and Notes

(1) de Gennes, P. G. *J. Chem. Phys.* **1971**, *55*, 572–579.
(2) Doi, M.; Edwards, S. F. *The Theory of Polymer Dynamics*; Oxford University Press: New York, 1986.
(3) Watanabe, H. *Prog. Polym. Sci.* **1999**, *24*, 1253–1403.
(4) McLeish, T. C. B. *Adv. Phys.* **2002**, *51*, 1379–1527.
(5) Dealy, J. M.; Larson, R. G. *Structure and Rheology of Molten Polymers*; Hanser Verlag: Munich, Germany, 2006.
(6) Ball, R. C.; McLeish, T. C. B. *Macromolecules* **1989**, *22*, 1911–1913.
(7) Marrucci, G. *J. Polym. Sci., Polym. Phys. Ed.* **1985**, *23*, 159–177.
(8) Milner, S. T.; McLeish, T. C. B. *Macromolecules* **1997**, *30*, 2159–2166.
(9) Milner, S. T.; McLeish, T. C. B. *Macromolecules* **1998**, *31*, 7479–7482.
(10) Frischknecht, A. L.; Milner, S. T. *Macromolecules* **2000**, *33*, 9764–9768.
(11) Frischknecht, A. L.; Milner, S. T.; Pryke, A.; Young, R. N.; Hawkins, R.; McLeish, T. C. B. *Macromolecules* **2002**, *35*, 4801–4820.
(12) McLeish, T. C. B.; Allgaier, J.; Bick, D. K.; Bishko, G.; Biswas, P.; Blackwell, R.; Blottiere, B.; Clarke, N.; Gibbs, B.; Groves, D. J.; Hakiki, A.; Heenan, R. K.; Johnson, J. M.; Kant, R.; Read, D. J.; Young, R. N. *Macromolecules* **1999**, *32*, 6734–6758.
(13) van Ruymbeke, E.; Bailly, C.; Keunings, R.; Vlassopoulos, D. *Macromolecules* **2006**, *39*, 6248–6259.
(14) van Ruymbeke, E.; Kapnistos, M.; Knauss, D. M.; Vlassopoulos, D. *Macromolecules* **2007**, *40*, 1713–1719.
(15) van Ruymbeke, E.; Orfanou, K.; Kapnistos, M.; Iatrou, H.; Pitsikalis, M.; Hadjichristidis, N.; Lohse, D. J.; Vlassopoulos, D. *Macromolecules* **2007**, *40*, 594159–52. Watanabe, H.; Matsumiya, Y.; van Ruymbeke, E.; Vlassopoulos, D.; Hadjichristidis, N. *Macromolecules* **2008**, *41*, 6110–6124.
(16) van Ruymbeke, E.; Muliawan, E. B.; Hatzikiriakos, S. G.; Watanabe, H.; Hirao, A.; Vlassopoulos, D. *J. Rheol.* **2010**, *54*, 643–662.
(17) Das, C.; Inkson, N. J.; Read, D. J.; Kelmanson, M. A.; McLeish, T. C. B. *J. Rheol.* **2006**, *50*, 207–234.
(18) Larson, R. G. *Macromolecules* **2001**, *34*, 4556–4571.
(19) Park, S. J.; Shanbhag, S.; Larson, R. G. *Rheol. Acta* **2005**, *44*, 319–330.
(20) van Ruymbeke, E.; Vlassopoulos, D.; Mierzwa, M.; Pakula, T.; Charalabidis, D.; Pitsikalis, M.; Hadjichristidis, N. *Macromolecules* **2010**, *43*, 4401–4411.
(21) Wang, Z.; Chen, X.; Larson, R. G. *J. Rheol.* **2010**, *54*, 223–260.
(22) Blackwell, R. J.; Harlen, O. G.; McLeish, T. C. B. *Macromolecules* **2001**, *34*, 2579–2596.
(23) Daniels, D. R.; McLeish, T. C. B.; Crosby, B. J.; Young, R. N.; Fernyhough, C. M. *Macromolecules* **2001**, *34*, 7025–7033.
(24) Inkson, N. J.; Graham, R. S.; McLeish, T. C. B.; Groves, D. J.; Fernyhough, C. M. *Macromolecules* **2006**, *39*, 4217–4227.
(25) Kapnistos, M.; Vlassopoulos, D.; Roovers, J.; Leal, L. G. *Macromolecules* **2005**, *38*, 7852–7862.

(26) Kapnistos, M.; Koutalas, G.; Hadjichristidis, N.; Roovers, J.; Lohse, D. J.; Vlassopoulos, D. *Rheol. Acta* **2006**, *46*, 273–286.
(27) Chambon, P.; Fernyhough, C. M.; Im, K.; Chang, T.; Das, C.; Embery, J.; McLeish, T. C. B.; Read, D. J. *Macromolecules* **2008**, *41*, 5869–5875.
(28) Kirkwood, K. M.; Leal, L. G.; Vlassopoulos, D.; Driva, P.; Hadjichristidis, N. *Macromolecules* **2009**, *42*, 9592–9608.
(29) Lee, J. H.; Driva, P.; Hadjichristidis, N.; Wright, P. J.; Rucker, S. P.; Lohse, D. J. *Macromolecules* **2009**, *42*, 1392–1399.
(30) Zhou, Q.; Larson, R. G. *Macromolecules* **2007**, *40*, 3443–3449.
(31) Zamponi, M.; Pyckhout-Hintzen, W.; Wischnewski, A.; Monkenbusch, M.; Willner, L.; Kali, G.; Richter, D. *Macromolecules* **2010**, *43*, 518–524.
(32) van Ruymbeke, E.; Keunings, R.; Bailly, C. *J. Non-Newtonian Fluid Mech.* **2005**, *128*, 7–22.
(33) Pattamaprom, C.; Larson, R. G. *Rheol. Acta* **2000**, *39*, 517–531.
(34) Pattamaprom, C.; Larson, R. G. *Rheol. Acta* **2001**, *40*, 516–532.
(35) Pattamaprom, C.; Larson, R. G.; Sirivant, A. *Rheol. Acta* **2008**, *47*, 689–700.
(36) van Ruymbeke, E.; Vlassopoulos, D.; Kapnistos, M.; Liu, C. Y.; Bailly, C. *Macromolecules* **2010**, *43*, 525–531.
(37) Roovers, J.; Graessley, W. W. *Macromolecules* **1981**, *14*, 766–773.
(38) Schwarzl, F. R. *Rheol. Acta* **1971**, *10*, 166–173.
(39) Roovers, J.; Toporowski, P. *Macromolecules* **1987**, *20*, 2300–2306.
(40) Milner, S. T.; McLeish, T. C. B.; Young, R. N.; Johnson, J.; Hakiki, A. *Macromolecules* **1998**, *31*, 9345–9353.
(41) Blottiere, B.; McLeish, T. C. B.; Hakiki, A.; Young, R. N.; Milner, S. T. *Macromolecules* **1998**, *31*, 9295–9304.
(42) Watanabe, H.; Ishida, S.; Matsumiya, Y.; Inoue, T. *Macromolecules* **2004**, *37*, 6619–6631.
(43) Watanabe, H.; Ishida, S.; Matsumiya, Y.; Inoue, T. *Macromolecules* **2004**, *37*, 1937–1951.
(44) Watanabe, H.; Matsumiya, Y.; Inoue, T. *Macromolecules* **2002**, *35*, 2339–2357.
(45) McLeish, T. C. B. *J. Rheol.* **2003**, *47*, 177–198.
(46) van Ruymbeke, E.; Balacca, L.; Coppola, S.; Righi, S.; Vlassopoulos, D. *J. Rheol.* **2010**, *54*, 507–538.
(47) Park, S. J.; Larson, R. G. *Macromolecules* **2004**, *37*, 597–604.
(48) Likhtman, A. E.; McLeish, T. *Macromolecules* **2002**, *35*, 6332–6343.
(49) Liu, C. Y.; He, J. S.; Keunings, R.; Bailly, C. *Macromolecules* **2006**, *39*, 3093–3097.
(50) Liu, C. Y.; Halasa, A. F.; Keunings, R.; Bailly, C. *Macromolecules* **2006**, *39*, 7415–7424.
(51) Larson, R. G.; Sridhar, T.; Leal, L. G.; McKinley, G. H.; Likhtman, A. E.; McLeish, T. C. B. *J. Rheol.* **2003**, *47*, 809–818.
(52) Liu, C. Y.; He, J. S.; van Ruymbeke, E.; Keunings, R.; Bailly, C. *Polymer* **2006**, *47*, 4461–4479.
(53) Fetters, L. J.; Lohse, D. J.; Colby, R. H. Chain Dimensions and Entanglement Spacing. In *Physical Properties of Polymers Handbook*, 2nd ed., Mark, J. E., Ed.; Springer: Berlin, 2007.
(54) Kapnistos, M.; Kirkwood, K. M.; Ramirez, J.; Vlassopoulos, D.; Leal, L. G. *J. Rheol.* **2009**, *53*, 1133–1153.